particles

MDPI

Article

Thickness and Color Structure of Center Vortices in Gluonic SU(2) QCD

Rudolf Golubich * and Manfried Faber

Atominstitut, Technische Universität Wien, 1020 Wien, Austria; faber@kph.tuwien.ac.at

* Correspondence: rudolf.golubich@gmail.com

Received: 30 April 2020; Accepted: 21 May 2020; Published: 22 May 2020



Abstract: In search for an effective model of quark confinement we study the vacuum of SU(2) quantum chromodynamic with lattice simulations using Wilson action. Assuming that center vortices are the relevant excitations causing confinement, we analyzed their physical size and their color structure. We present confirmations for a vanishing thickness of center vortices in the continuum limit and hints at their color structure. This is the first time that algorithms for the detection of thick center vortices based on non-trivial center regions has been used.

Keywords: quantum chromodynamics; confinement; center vortex model; vacuum structure

PACS: 11.15.Ha; 12.38.Gc

1. Introduction

The strong interaction relevant for quantum chromodynamic is governed by an SU(3) symmetric Lagrangian. One of the most important non-perturbative properties of QCD is confinement. It results from a non-perturbative vacuum. This raises the question about the corresponding non-perturbative degrees of freedom. The center vortex model [1,2] is based on the idea that the important ingredients are center degrees of freedom in the form of closed magnetic flux tubes, quantised to the two non-trivial center elements of SU(3). In this first study of the detection of finite center regions, we are investigating SU(2)-QCD which is also confining and breaks chiral symmetry dynamically [3]. It has only one non-trivial center element and one species of magnetic flux tubes. Working with the Wilson action, the lattice spacing is adjusted by choosing the inverse coupling β, which is related to the coupling constant g by $\beta = 4/g^2$. In this type of studies the closed color magnetic flux lines percolating the vacuum, are located by P-vortices [4], identified in the direct maximal center gauge, which aims at finding gauge matrices $\Omega(x)$ so that

$$\acute{U}_\mu(x) = \Omega(x) U_\mu(x) \Omega^\dagger(x + e_\mu) \text{ maximizes } R^2_{SA} = \sum_x \sum_\mu \mid \mathrm{Tr}[\acute{U}_\mu(x)] \mid^2, \tag{1}$$

with $U_\mu(x)$, an element of SU(2), being the gluonic link variable at lattice point x in direction μ. We chose the gauge by a modified simulated annealing procedure preserving non-trivial center regions, regions whose perimeter evaluates to a non-trivial center element. This is done by rejecting transformations that after center projection would result in the vanishing of non-trivial center regions [5]. The details are described in ref. [6]. As long as non-trivial center regions vanish we keep the simulated annealing temperature high.

Plaquettes pierced by a P-vortex are found by projection onto the central degrees of freedom, in SU(2) just a sign,

$$Z_\mu(x) = \text{sign Tr}[\acute{U}_\mu(x)]. \tag{2}$$

They evaluate to the non-trivial center element in the projected configuration. The vortex detection can be seen as a best fit procedure of a thin vortex configuration to a given field configuration [4,7], see Figure 1: gauge dependent P-vortices of singular thickness locate gauge independent thick vortices of finite thickness [8].

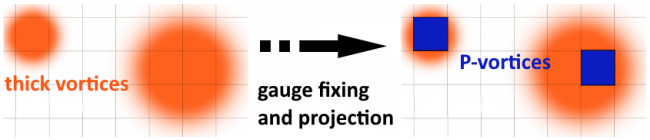


Figure 1. Vortex detection as a best fit procedure of P-vortices to thick vortices shown in a two dimensional slice through a four dimensional lattice.

Center projection leads to plaquettes with non-trivial center values. The P-plaquettes form P-vortices, closed surfaces in dual space; see Figure 2. We relate the thickness d_{vort} of the vortex to the area A of the cross section by $d_{vort} \propto \sqrt{A}$.

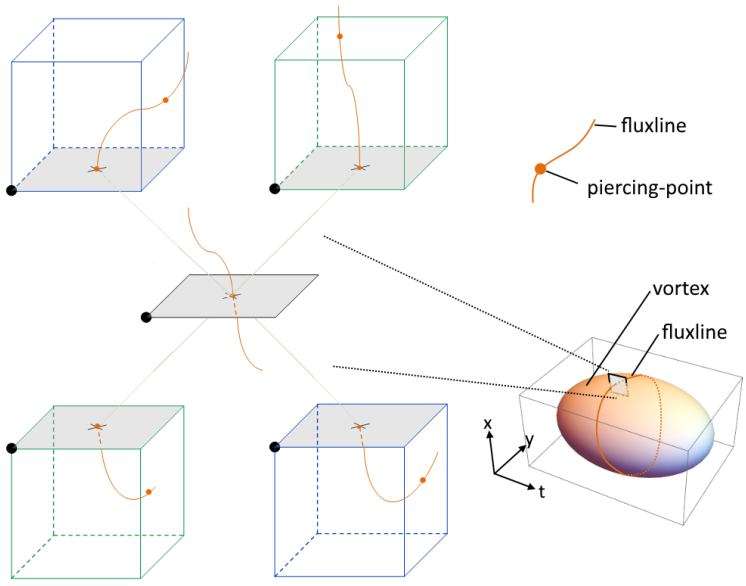


Figure 2. A closed color magnetic flux evolving in time creates a closed surface in four dimensional spacetime. On the lattice a flux piercing a plaquette has to be traceable through the four attached cubes.

Assuming independence of vortex piercings, the vortex density ϱ_{vort}, the number of P-plaquettes per unit volume, is related to the string tension σ by

$$\sigma = -\ln(1 - 2 * \varrho_{vort}). \tag{3}$$

Correlations of such piercings lead to an overestimation of σ. To reduce the amount of such short range fluctuations, smoothing procedures of the vortex surface are used [9]. A determination of σ, more independent from short range fluctuations is given using $R \times T$ Wilson loops $W(R,T)$ by the Creuz ratios

$$\chi(R,T) = -\ln \frac{\langle W(R+1,T+1)\rangle \, \langle W(R,T)\rangle}{\langle W(R,T+1)\rangle \, \langle W(R+1,T)\rangle}, \tag{4}$$

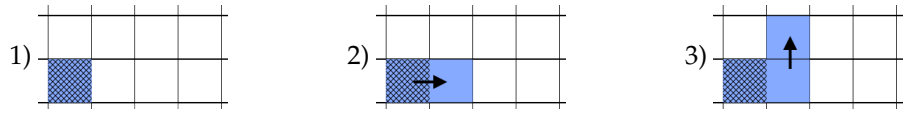
Comparing the Creutz ratios we can assure that the center projected configuration and the full configuration have the same lattice spacing and that the center projection captures the full string tension. The lattice spacing is defined via the physical value of the string tension $\sigma_{\mathrm{ph}} = (440\ \mathrm{MeV})^2$ and calculates the string tension in lattice units, $\sigma_{lattice}$, to

$$a = \sqrt{\sigma_{lattice}} * \frac{197}{440}\ \mathrm{fm}. \tag{5}$$

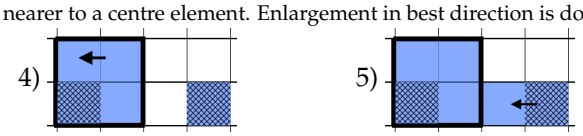
For the first time we present results based on our algorithms for locating thick vortices. We get indications for a vanishing thickness of center vortices in the continuum limit, which is compatible with the findings in [10]. In addition, we found hints of a color structure on the vortex surface.

2. Materials and Methods

After gauge fixing to direct maximal center gauge preserving non-trivial center regions during simulated annealing with up to 2700 steps, we identify P-plaquettes in the $Z_\mu(x)-$configurations. We check how good we capture the confining excitations by calculating the Creutz ratios. Our algorithm detects non-trivial center regions by the identification of loops enclosing thick vortices in the $U_\mu(x)-$configuration: starting with the full plaquette matrices $U_\Box(x)$ at the position of the identified P-plaquettes, the loop forming the plaquette is enlarged by pushing its perimeter outwards over neighboring plaquettes so that the path integrated product of the enlarged region gets closer to the non trivial center element; see Figure 3.



Steps 1-3: Starting with a P-plaquette it is tested, which enlargement around a neighbouring plaquette brings the regions evaluation nearer to a centre element. Enlargement in best direction is done.



Steps 4-5: When no more enlargement results to an improvement of the regions evaluation, the perimeter of the region is stored and another P-plaquette is taken for a new enlargement procedure.

Figure 3. Thick vortex piercings are identified by detecting non-trivial center regions around P-plaquettes, plaquettes pierced by P-vortices.

When all minimal planar loops are identified that enclose the thick vortex, its thickness can be estimated by counting the number of enclosed plaquettes. We take care of the scaling of the lattice spacing a and fit the cross section $A(a)$ of the piercing by

$$A(a) \;=\; A_0 \;+\; k_A * a \;+ c_A * a^2, \tag{6}$$

with fit-parameters k and c. With the diagrams in the lower row of Figure 4, we want to show that the term quadratic in a detects whether cross sections have contributions proportional to the plaquette area. The term proportional a results from the finite resolution of the boundary; see the upper row of Figure 4. The constant term A_0 indicates the predicted size of the physical area in the continuum limit.

To study the color structure of the vacuum, a quantity measuring the homogeneity of the flux building up the vortex is needed. The concept was first presented in [11] and consists of referencing different plaquettes to the same lattice point; see Figure 5.

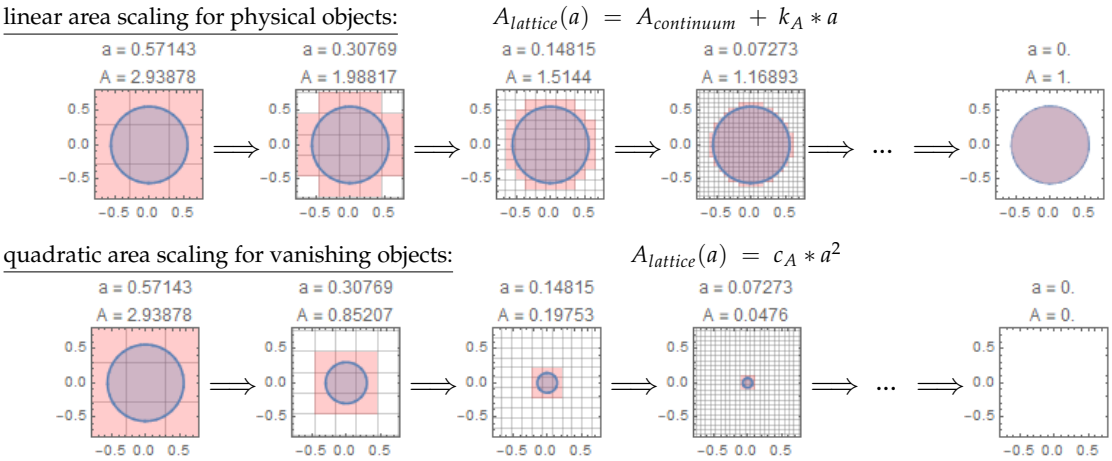


Figure 4. When measuring the area $A_{continuum}$ of a physical object piercing a plane in our toy lattice world, due to the pixel size a linear dependence on the lattice constant a is expected, as depicted in the upper part. Objects with cross sections proportional to plaquette areas lead to contributions of the order a^2.

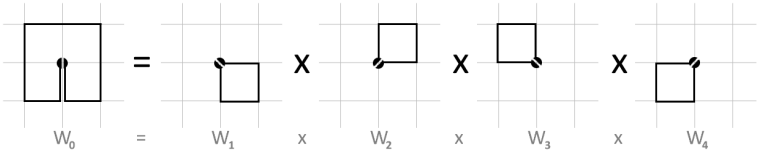


Figure 5. To measure the color homogeneity of a 2×2-loop its four plaquettes are referenced to the central lattice point of the 2×2-loop.

By factorizing the plaquettes W_i into Pauli matrices σ_j,

$$W_j \;=\; \cos(\alpha_j)\;\sigma_0 + \mathrm{i}\sum_{k=1}^{3}\;\sin(\alpha_j)\;(n_j)_k\;\sigma_k,\;\text{with}\;n_j \in \mathbb{S}^2,\;\mid n_j \mid = 1, \tag{7}$$

we define the *S2-homogeneity* of m plaquettes referenced to the same lattice point using the $\mathbb{S}^2$ vectors n_j as

$$h_{S2} \;:=\; \frac{1}{m}\mid \sum_{j=1}^{m} n_j \mid \in [0,1]. \tag{8}$$

In this work we will only compare two plaquettes for calculating h_{S2} ($m = 2$ in Equation (8)) because this allows to clearly distinguish different properties as is shown in the next section. We assume a scaling dependency with the lattice spacing a of the form

$$h_{S2} \;=\; h_{CS2} + k_h * \frac{a}{\mathrm{fm}} + c_h * \frac{a^2}{\mathrm{fm}^2} + \mathcal{O}(\frac{a^3}{\mathrm{fm}^3}) \tag{9}$$

and fit h_{CS2}, k_h and c_h to the data h_{S2} taken from the lattice. The value of h_{CS2} corresponds to the continuum limit of the color homogeneity. The S2-homogeneity of plaquettes at position x and $x + \hat{\mu}$ with $\mid \hat{\mu} \mid = a$ can be related to the difference

$$\Delta n \;:=\; \mid n(x+\hat{\mu}) - n(x) \mid = 2\sqrt{1 - h_{S2}^2} \Rightarrow dn \;=\; 2\sqrt{1 - h_{CS2}^2}. \tag{10}$$

With given color vector $n_1 \;=\; n(x)$, the second vector $n_2 \;=\; n(x+\hat{\mu})$ is only fixed to the cone shown in Figure 6.

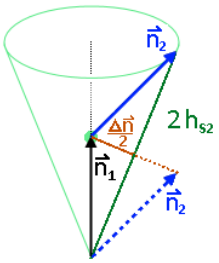


Figure 6. By Equation (10) the S2-homogeneity h_{S2} of two color vectors n_1 and n_2 is related to the norm $\Delta n = \mid n_2 - n_1 \mid$.

The sign of k indicates whether we have long or short ranged fluctuations.

$$\Delta^2 n \approx -\frac{2h_{S2}}{\sqrt{1 - h_{CS2}^2}} * k_h. \tag{11}$$

Negative k indicates, that the Δn increases with growing distance between the considered color vectors and positive k_h implies decreasing Δn with growing distance; see Figure 7.

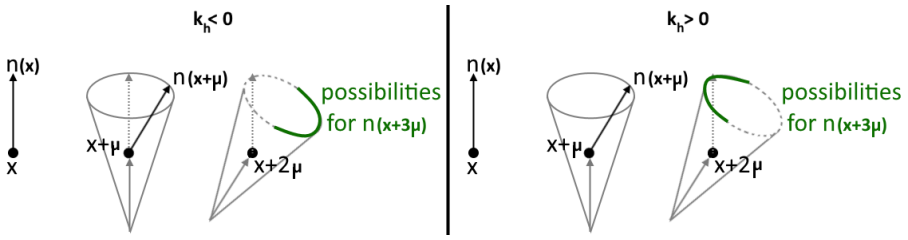


Figure 7. Starting from a lattice point x with corresponding color vector $n(x)$, the S2-homogeneity gives information about the neighbouring color vectors. The sign of k can be represented geometrically, as is depicted above. The left part can be interpreted as long range fluctuations of n-vectors, the right side as short range fluctuations of n-vectors.

For an analysis of a geometric structure we need to define some terms, distinguishing different orientations and positions of pairs of plaquettes in spacetime. By calculating the S2-homogeneity of two neighboring plaquettes in the same plane in spacetime we can distinguish four "planar" color homogeneities:

- Inside the thick vortex ("Interior"): both plaquettes lying within the loop;
- Outside the thick vortex ("Outside"): both plaquettes lying outside the loop;
- On the vortex edge ("Edge"): one plaquette within and one outside the thick vortex;
- Average over the whole lattice ("Vacuum"): no further criteria.

Two non-planar plaquettes are considered "longitudinal" if they belong to the same cube, see Figure 2 and therefore can be pierced by the same flux line. For two such non-planar plaquettes it is not necessary that they are of same direction and we distinguish four relative positions in order to study the corresponding S2-homogeneities:

- Along the vortex flux ("online"): both plaquettes are P-plaquettes;
- Outside the vortex ("offline"): non of the plaquettes is a P-plaquette;
- Trespassing the vortex ("leaving"): only one of the two plaquettes is a P-plaquette;
- Average over the whole lattice ("Vacuum"): no criteria.

Figure 8 tries to clarify the idea behind these planar and longitudinal properties. The S2-homogeneities of planar and longitudinal vacuum can deviate because the distance of the compared plaquettes is not necessarily identical.

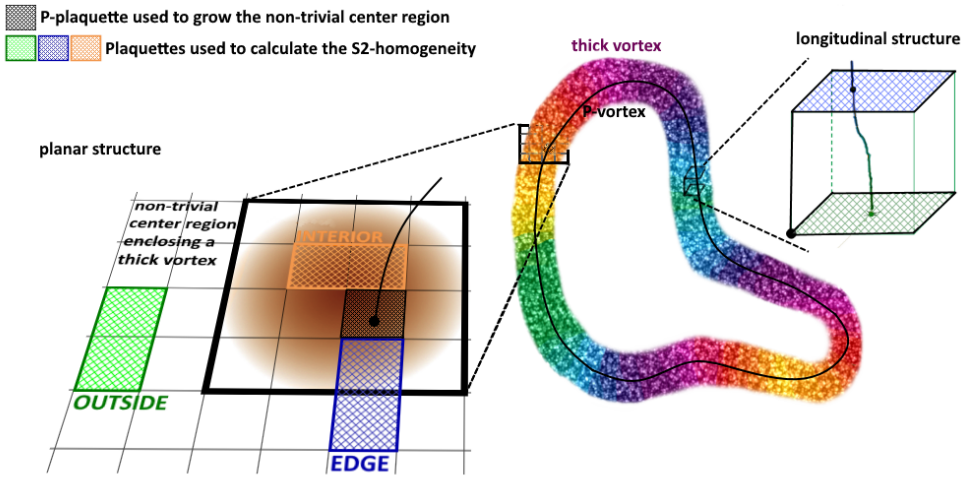


Figure 8. The colorful thick line in the middle of the figure represents flux building a thick vortex and the black thin line in its center indicates the fluxline of the corresponding P-vortex. On the non-projected field configuration this vortex is detected by the non-trivial center region, surrounded by a black rectangle on the original lattice in the left diagram. We investigate the S2-homogeneity on the pairs of plaquettes, outside the vortex, inside the vortex and on its edge, indicated there by shaded regions. With pairs of non-planar plaquettes, depicted in the right diagram, an analysis of the longitudinal color structure is possible.

As calculations of the lattice spacing require much more statistics than we need for the calculations of the piercing area and the color structure, we do a cubic interpolation of the literature values given in Table 1 to determine the lattice spacing.

Table 1. The values of the lattice spacing in fm and the string tension corresponding to the respective value of β are based on [12–16] by setting the physical string tension to $(440\ \mathrm{MeV})^2$.

β	**2.3**	**2.4**	**2.5**	**2.635**	**2.74**	**2.85**
a [fm]	0.165(1)	0.1191(9)	0.0837(4)	0.05409(4)	0.04078(9)	0.0296(3)
σ [lattice]	0.136(2)	0.071(1)	0.0350(4)	0.01459(2)	0.0.00830(4)	0.00438(8)

Our calculations cover an interval from $\beta = 2.1$ to $\beta = 2.55$ in steps of 0.05. To each value of β we generate 120 configurations with Wilson action, respectively, 10 for lattices of size 14^4 and 16^4 and 100 for lattices of size 18^4. By calculating the string tension via Creutz ratios χ in the center projected configuration and comparing with the literature values we can quantify how good we detected the center vortices and by approximating the string tension via the vortex density ϱ_{vort} we can check how many short range fluctuations perturb our analysis. As can be seen in Figure 9, our identification of the excitations relevant for confinement are quite satisfactory for the middle β-regime, although slightly underestimate the literature values in the lower β regime and slightly overestimate it for higher β. We accept an overestimated vortex density in order not to overlook excitations relevant for confinement when reconstructing thick vortices.

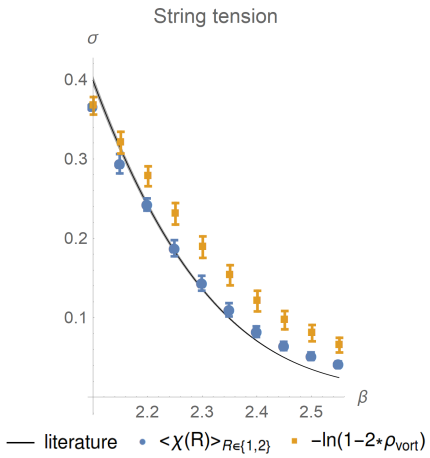


Figure 9. Comparison of the string tension calculated via Creutz ratios in the projected configuration and calculations based on the vortex density with the literature values.

3. Results

Figure 10 shows our results and fits with extrapolations to the continuum limit. All parameters of the respective fits are shown with full value and standard error in the tables below. The T-statistic and *P*-value are shown to check the quality of the fit. First we present indications for a vanishing thickness of vortices in the continuum limit, then we discuss their color structure.

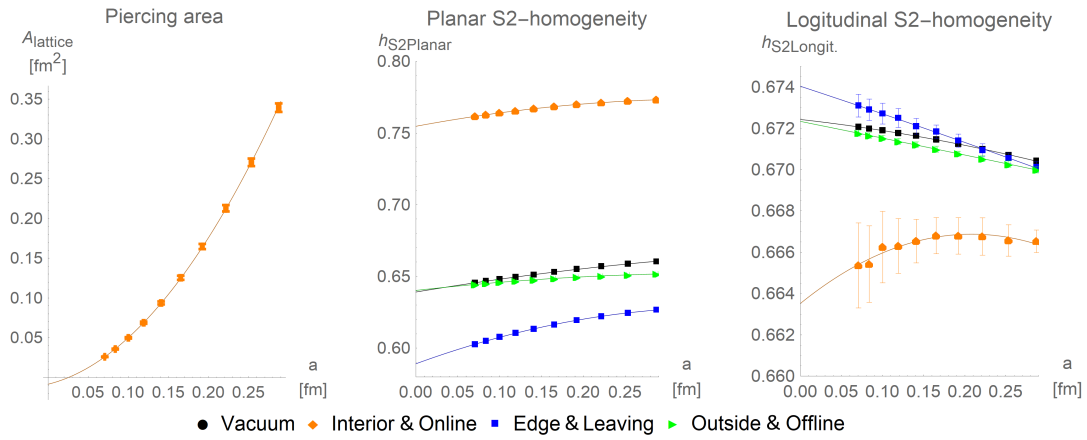


Figure 10. The data of vortex thickness (**left**), planar S2-homogeneity (**middle**) and longitudinal S2-homogeneity (**right**) are shown in dependence of the lattice spacing a. The homogeneities are distinguished for vortex interior, vortex edge, vortex outside and the average over the whole volume of the lattice (vacuum). All three diagrams indicate a vanishing vortex thickness. From the data in the middle and the right diagram we conclude that the vortex is inhomogeneous in longitudinal direction, but homogeneous in planar directions.

In the left part of Figure 10 and in Table 2 the dominance of the quadratic term with factor $c_A = 3.4(2)$ over the linear factor $k_A = 0.25(5)$ fm and the small non-physical negative value of $A_{continuum} = -0.009(3)$ fm^2 for the piercing area indicate a vanishing vortex thickness in the continuum, remember Figure 4. This is also strengthened by the fact, that within errors we find equal continuum extrapolations of S2-homogeneities for the vacua and outside and offline the vortex, see green and black line corresponding to Outside AND Offline and Vacuum in the middle and right of Figure 10. In the continuum limit the planar homogeneity (middle) of the vacuum of $h_{CS2} = 0.639(2)$ is compatible to the planar homogeneity outside the vortex $h_{CS2} = 0.640(2)$; see Table 3. The longitudinal homogeneity (right) of the vacuum of $h_{CS2} = 0.672(1)$ is compatible to the longitudinal homogeneity *offline* the vortex $h_{CS2} = 0.672(1)$; see Table 4. Furthermore, the factors k_h of the linear terms are compatible for the whole vacuum (planar $k_h = 0.097(27)$, longitudinal $k_h = 0.00(2)$) and outside/offline the vortex (planar $k_h = 0.065(27)$, longitudinal $k_h = 0.00(2)$).

Table 2. The parameters of fitting $A_{lattice}(a) = A_{continuum} + k_A * a + c_A * a^2$ to the measured vortex piercing area on the lattice. The dominance of the quadratic factor c_A over the linear factor k_A and the near to zero value of $A_{continuum}$ indicate a vanishing vortex thickness in the continuum.

Piercing Area	Estimate	Standard Error	t-Statistic	*P*-Value
$A_{continuum}$/fm^2	−0.00855142	0.00281233	−3.04069	0.0188287
k_A/fm	0.248823	0.0489884	5.07922	0.00143227
c_A	3.3713	0.174175	19.3559	2.44947×10^{-7}

Within errors the quadratic factors for the vacuum (planar $c_h = -0.08(8)$ and longitudinal $c_h = -0.01(8)$) are identical to those outside/offline the vortex (planar $c_h = -0.09(9)$ and longitudinal $c_h = 0.00(8)$). This is compatible to the assumption, that the two volumina, that is, whole vacuum and outside/offline the vortex, coincide.

Table 3. The parameters of fitting $h_{S2} = h_{CS2} + k_h * \frac{a}{\text{fm}} + c_h * \frac{a^2}{\text{fm}^2} + \mathcal{O}(a^3)$ to the planar color homogeneity of the vacuum and the vortex outside. The three parameters are identical within errors for the vacuum and the vortex outside. The positive sign of k_h indicates the absence of long range fluctuations of the n-vector.

Planar Vacuum	**Estimate**	**Standard Error**	**t-Statistic**	***P*-Value**
h_{CS2}	0.639146	0.00173019	369.407	2.81298×10^{-16}
k_h	0.0972656	0.0270039	3.60191	0.00871761
c_h	−0.0783918	0.0851997	−0.920096	0.38813
Planar Outside	**Estimate**	**Standard Error**	**t-Statistic**	***P*-Value**
h_{CS2}	0.640275	0.00178975	357.745	3.52117×10^{-16}
k_h	0.0652618	0.0276802	2.3577	0.0505116
c_h	−0.0886687	0.0868844	−1.02054	0.341442

In Table 3 the two positive signs of the k_h and the two small values of the c_h outside the vortex and for the vacuum indicate that there are no long range fluctuations (remember Figure 7) of the color vector, although the high P-values demand caution with this interpretation.

Table 4. The parameters of fitting $h_{S2} = h_{CS2} + k_h * \frac{a}{\text{fm}} + c_h * \frac{a^2}{\text{fm}^2} + \mathcal{O}(a^3)$ to the longitudinal color homogeneity of the vacuum and offline the vortex. The three parameters are identical within errors for the vacuum and offline. k_h vanishes within errors, the negative sign would indicate the absence of long range fluctuations of the color vector.

Longitudinal Vacuum	**Estimate**	**Standard Error**	**t-Statistic**	***P*-Value**
h_{CS2}	0.672431	0.00149354	450.226	7.04231×10^{-17}
k_h	−0.00447137	0.0244568	−0.182827	0.860116
c_h	−0.00892278	0.0789767	−0.11298	0.913218
Longitudinal Offline	**Estimate**	**Standard Error**	**t-Statistic**	***P*-Value**
h_{CS2}	0.672338	0.00149817	448.773	7.20344×10^{-17}
k_h	−0.00806252	0.0245051	−0.329013	0.75177
c_h	−0.000394962	0.0790972	−0.00499337	0.996155

The high planar S2-homogeneity of $h_{CS2} = 0.755(3)$ within the vortex, compared to the vacuum value of $0.639(2)$ (see Tables 3 and 5) are also in favour of a vanishing vortex thickness; as a singular vortex can not have planar structure, a high planar S2-homogeneity inside the vortex cross section is expected.

Table 5. The parameters of fitting $h_{S2} = h_{CS2} + k_h * \frac{a}{\text{fm}} + c_h * \frac{a^2}{\text{fm}^2} + \mathcal{O}(a^3)$ to the planar color homogeneity of the vortex interior. h_{CS2} inside the vortex is clearly higher, than on the vortex edge, outside or in the whole vacuum (compare to Table 3).

Planar Interior	**Estimate**	**Standard Error**	**t-Statistic**	***P*-Value**
h_{CS2}	0.754742	0.00271182	278.316	2.04121×10^{-15}
k_h	0.108942	0.0378669	2.87697	0.0237542
c_h	−0.155359	0.112538	−1.38049	0.209904

The positive value of $k_h = 0.12(4)$ inside this piercing area indicates that the planar homogeneity of the vortex is disturbed only by short range fluctuations (remember Figure 8) of the color vector, which is again in favor of a non existing planar color structure, hence vanishing thickness of the vortex.

On the vortex edge the planar S2-homogeneity with a value of $h_{CS2} = 0.589(2)$ is below the vacuum; compare Table 6 to Table 3.

Table 6. The parameters of fitting $h_{S2} = h_{CS2} + k_h * \frac{a}{\text{fm}} + c_h * \frac{a^2}{\text{fm}^2} + \mathcal{O}(a^3)$ to the vortex edge. h_{CS2} on the vortex edge is lower than the vacuum value, compare to Table 3. The positive value of k_h and the non-vanishing value of c_h indicate a strong fluctuation of the color vector in short range when trespassing the vortex surface.

Planar Edge	Estimate	Standard Error	t-Statistic	*P*-Value
h_{CS2}	0.589117	0.00249172	236.43	6.39273×10^{-15}
k_h	0.21375	0.0354255	6.03378	0.00052433
c_h	−0.290042	0.106036	−2.73532	0.0291143

The positive value of $k_h = 0.21(4)$ and the non-vanishing value of $c_h = -0.3(1)$ at the vortex edge indicate a big difference of the color vector inside and outside of the non-trivial center regions.

The longitudinal measurement depicted on the right side of Figure 10 shows that the color vector fluctuates strongly along the vortex surface. Comparing Table 7 to Table 4, the longitudinal S2-homogeneity of $h_{CS2} = 0.664(4)$ along the vortex is below the vacuum value of $0.672(1)$. This hints at a non-trivial, longitudinal color structure of the vortex surface. The positive value of $k_h = 0.03(5)$ along the vortex line (online) indicates long range fluctuations of the color vector, but to exclude a negative value more data has to be collected. Furthermore, the value of $c_h = -0.1(1)$ along the vortex requires more statistics. A fit up to quadratic order might not be the optimum for the color homogeneity along the vortex, possible is also a linear raise with increasing lattice spacing until saturation is reached. As of that, the error of h_{CS2} along the vortex might be underestimated by the fit. Of interest is further, that the longitudinal S2-homogeneity leaving, that is, one plaquette being pierced by the vortex and one not, with a value of $h_{CS2} = 0.674(2)$ is slightly above the homogeneity of the surrounding vacuum, compare Table 8 to Table 4.

Table 7. The parameters of fitting $h_{S2} = h_{CS2} + k_h * \frac{a}{\text{fm}} + c_h * \frac{a^2}{\text{fm}^2} + \mathcal{O}(a^3)$ to the longitudinal color homogeneity online the vortex. Comparing the value for h_{S2} along the vortex with the value of the vacuum in Table 4, the color vector fluctuates strongly along the vortex.

Longitudinal Online	Estimate	Standard Error	t-Statistic	*P*-Value
h_{CS2}	0.663525	0.00397127	167.081	7.26006×10^{-14}
k_h	0.0322137	0.0492818	0.653662	0.534205
c_h	−0.077377	0.136902	−0.565202	0.589584

Table 8. The parameters of fitting $h_{S2} = h_{CS2} + k_h * \frac{a}{\text{fm}} + c_h * \frac{a^2}{\text{fm}^2} + \mathcal{O}(a^3)$ to the longitudinal color homogeneity leaving the vortex.

Longitudinal Leaving	Estimate	Standard Error	t-Statistic	*P*-Value
h_{CS2}	0.67404	0.00201668	334.233	5.66693×10^{-16}
k_h	−0.013139	0.0300097	−0.437827	0.674703
c_h	−0.0023116	0.0923786	−0.0250231	0.980735

The longitudinal S2-homogeneity online is calculated solely on P-plaquettes, but the thick vortex spans over several plaquettes. We know that this measurement oversees neighboring plaquettes that belong to the thick vortex.

4. Discussion

We have presented strong evidence for a vanishing thickness of SU(2) center vortices in the continuum limit and indications for a longitudinal color structure of the vortex surface: along the vortex and when trespassing the vortex surface the fluctuations of the color vectors are stronger than in the surrounding vacuum. Our data favor a model of surface like vortices of thickness vanishing in the continuum limit with non-trivial color structure reflected by the behavior of the longitudinal S2-homogeneity h_{S2} along the flux lines building up the surface. Fluctuations of the color vector $\vec{n}$ covering the whole $\mathcal{S}^2$ along the vortex surface could further lead to a topological charge [17–19]. When projecting the $\mathcal{S}^2$ color vectors to a given axis defined by an abelian subgroup, we get positive and negative regions separated by world lines of magnetic monopoles.

The vanishing vortex thickness in the continuum limit hints at infinitely thin strings populating the vacuum. The corresponding action diverges and has to be canceled by an entropic contribution [10]. The longitudinal color structure relates center vortices to abelian monopoles. For them, corresponding divergences have been reported in ref. [20]. The question arises if the vanishing thickness of the vortex in the continuum limit influences the representation dependence of the string tension.

To reduce the errors of our data concerning the color structure of vortices, we will collect more data. This might allow to quantify the spatial extent of the color fluctuations along the vortex surface. In the errors indicated in all tables and figures, we haven also taken into account the error of the literature value of the lattice spacing a as given in Table 2. This puts an lower limit of 0.0014 to the errors of the S2-homogeneities. Our results concern the longitudinal S2-homogeneity with respect to P-plaquettes. By further taking into account the plaquettes building up non-trivial center regions, an increase in the statistics by a factor of the size of non-trivial center regions could be achieved for vortex concerning data.

Our studies show that the S2-homogeneity is useful for analyzing the color structure of the vacuum and pave the way for further work. It would be interesting to generalize our procedures to SU(3). As this group has two non-trivial center elements, the algorithms for detecting non-trivial center regions need to be modified to enlarge regions with respect to the two non-trivial center elements. Running the enlargement algorithms for the two different non-trivial center elements separately allows overlaps. This could be prevented by modifying the criteria for enlargement. The gauge fixing procedure based on simulated annealing can be implemented for SU(3) without modifications. It may be problematic that our implementation is quite memory-intensive, requiring contiguous memory. As a generalization to SU(3) would further increases the memory requirements it might be favorable to look for a memory-optimized implementation of our algorithms.

Author Contributions: Conceptualization, R.G.; Software, R.G.; Supervision, M.F.; Visualization, R.G.; Writing – original draft, R.G.; Writing – review and editing, M.F. All authors have read and agreed to the published version of the manuscript.

Funding: This research received no external funding.

Conflicts of Interest: The authors declare no conflict of interest.

References

1. 't Hooft, G. On the phase transition towards permanent quark confinement. *Nucl. Phys. B* **1978**, *138*, 1–25. [CrossRef]
2. Cornwall, J.M. Quark confinement and vortices in massive gauge-invariant QCD. *Nucl. Phys. B* **1979**, *157*, 392–412. [CrossRef]
3. Faber, M.; Höllwieser, R. Chiral symmetry breaking on the lattice. *Prog. Part. Nucl. Phys.* **2017**, *97*, 312–355. [CrossRef]

4. Del Debbio, L.; Faber, M.; Giedt, J.; Greensite, J.; Olejnik, S. Detection of center vortices in the lattice Yang-Mills vacuum. *Phys. Rev.* **1998**, *D58*, 094501, [CrossRef]
5. Golubich, R.; Faber, M. Center regions as a solution to the Gribov problem of the center vortex model. *Acta Phys. Pol. B Proc. Suppl.* **2020**, in press. [CrossRef]
6. Golubich, R.; Faber, M. Improving Center Vortex Detection by Usage of Center Regions as Guidance for the Direct Maximal Center Gauge. *Particles* **2019**, *4*, 30. [CrossRef]
7. Faber, M.; Greensite, J.; Olejnik, S. Direct Laplacian center gauge. *JHEP* **2001**, *11*, 053. [CrossRef]
8. Del Debbio, L.; Faber, M.; Greensite, J.; Olejnik, S. Center dominance and Z(2) vortices in SU(2) lattice gauge theory. *Phys. Rev. D* **1997**, *55*, 2298–2306, [CrossRef]
9. Bertle, R.; Faber, M.; Greensite, J.; Olejnik, S. The Structure of Projected Center Vortices in Lattice Gauge Theory. *J. High Energy Phys.* **1999**. [CrossRef]
10. Gubarev, F.; Kovalenko, A.; Polikarpov, M.; Syritsyn, S.; Zakharov, V. Fine tuned vortices in lattice SU(2) gluodynamics. *Phys. Lett. B* **2003**, *574*, 136–140, [CrossRef]
11. Golubich, R.; Faber, M. Vortex Model of the QCD-vacuum—Successes and Problems. *Acta Phys. Pol. B Proc. Suppl.* **2018**. [CrossRef]
12. Bali, G.S.; Schlichter, C.; Schilling, K. Observing long color flux tubes in SU(2) lattice gauge theory. *Phys. Rev. D* **1995**, *51*, 5165–5198. [CrossRef] [PubMed]
13. Booth, S.P.; Hulsebos, A.; Irving, A.C.; McKerrell, A.; Michael, C.; Spencer, P.S.; Stephenson, P.W. SU(2) potentials from large lattices. *Nucl. Phys.* **1993**, *B394*, 509–526. [CrossRef]
14. Michael, C.; Teper, M. Towards the Continuum Limit of SU(2) Lattice Gauge Theory. *Phys. Lett.* **1987**, *B199*, 95–100. [CrossRef]
15. Perantonis, S.; Huntley, A.; Michael, C. Static Potentials From Pure SU(2) Lattice Gauge Theory. *Nucl. Phys.* **1989**, *B326*, 544–556. [CrossRef]
16. Bali, G.S.; Fingberg, J.; Heller, U.M.; Karsch, F.; Schilling, K. The Spatial string tension in the deconfined phase of the (3+1)-dimensional SU(2) gauge theory. *Phys. Rev. Lett.* **1993**, *71*, 3059–3062. [CrossRef] [PubMed]
17. Höllwieser, R.; Schweigler, T.; Faber, M.; Heller, U.M. Center vortices and topological charge. *PoS* **2012**, *ConfinementX*, 078.
18. Schweigler, T.; Höllwieser, R.; Faber, M.; Heller, U.M. Colorful SU(2) center vortices in the continuum and on the lattice. *Phys. Rev.* **2013**, *D87*, 054504. [CrossRef]
19. Höllwieser, R.; Schweigler, T.; Faber, M.; Heller, U.M. Center Vortices and Chiral Symmetry Breaking in SU(2) Lattice Gauge Theory. *Phys. Rev.* **2013**, *D88*, 114505. [CrossRef]
20. Zakharov, V. Hidden mass hierarchy in QCD. In Proceedings of the 8th Adriatic Meeting and Central European Symposia on Particle Physics in the New Millennium, Dubrovnik, Croatia, 4–14 September 2001.



© 2020 by the authors. Licensee MDPI, Basel, Switzerland. This article is an open access article distributed under the terms and conditions of the Creative Commons Attribution (CC BY) license (http://creativecommons.org/licenses/by/4.0/).